Crystal structure prediction of $LiBeH_3$ using *ab initio* total-energy calculations and evolutionary simulations

Chao-Hao Hu,[1,2,a)] A. R. Oganov,[3,4] Y. M. Wang,[5] H. Y. Zhou,[2] A. Lyakhov,[3] and J. Hafner[6]

[1]*Direction Chimie et Physico-chimie Appliquées, Institut Français du Pétrole, 1 and 4 Av. de Bois-Préau, 92852 Rueil-Malmaison Cedex, France*
[2]*Department of Information Materials Science and Engineering, Guilin University of Electronic Technology, Guangxi 541004, People's Republic of China*
[3]*Department of Materials, Laboratory of Crystallography, ETH Zürich, 8093 Zürich, Switzerland*
[4]*Department of Geology, Moscow State University, 119992 Moscow, Russia*
[5]*Shenyang National Laboratory for Materials Science, Institute of Metal Research, Chinese Academy of Sciences, 72 Wenhua Road, Shenyang 110016, People's Republic of China*
[6]*Fakultät für Physik and Center for Computational Materials Science, Universität Wien, Sensengasse 8/12, A-1090 Wien, Austria*

(Received 24 July 2008; accepted 14 October 2008; published online 18 December 2008)

The stable crystal structure of $LiBeH_3$ is predicted on the basis of *ab initio* total-energy calculations using density-functional theory and an extended database of candidate structures and using global optimizations based on an evolutionary algorithm. At the level of density-functional theory, a $CaSiO_3$_1-type structure with space group $P2_1/c$, containing BeH_4 tetrahedra linked in chains, is the ground-state structure of $LiBeH_3$ (α-$LiBeH_3$). It is found to be lower in energy than the structures proposed in previous studies. The analysis of the electronic structure shows that α-$LiBeH_3$ is an insulator with a band gap of about 4.84 eV and exhibits strong covalent bonding in the BeH_4 tetrahedral complexes. Calculations at finite temperatures and high pressures suggest that at $T=408$ K and ambient pressure a structural transition from α-$LiBeH_3$ ($CaSiO_3$-type) to a YBO_3-type structure with space group *Cmcm* occurs and that at a pressure of 7.1 GPa α-$LiBeH_3$ undergoes a pressure-induced structural transition from the α-phase to a $MgSiO_3$-type structure with space group $C2/c$. The calculated enthalpies of formation (−45.36 and −30.12 kJ/mol H_2 without and with zero-point energy corrections) are in good agreement with the experimental result, indicating that $LiBeH_3$ is a potential hydrogen storage material with low activation barriers for hydrogen desorption. © *2008 American Institute of Physics*. [DOI: 10.1063/1.3021079]

I. INTRODUCTION

Exploring sustainable hydrogen storage materials for mobile applications is still a scientific and technical challenge.[1] Much interest has been focused on the complex hydrides of light elements due to their high gravimetric hydrogen density (GHD).[2–5] However, due to their poor kinetics of hydrogenation and dehydrogenation reactions, these complex hydrides have been considered to be nonreversible energy storage materials for a long time. They have attracted much attention again in recent years since Bogdanovic and Schwickardi[2] found that the doping of $NaAlH_4$ with selected transition metals (Ti, Zr, Fe, etc.) can increase the rates of adsorption and desorption of hydrogen at moderate conditions. At present, however, the maximum material (not system) gravimetric capacity of 5.5 wt % H achieved for $NaAlH_4$ still does not meet the target of 6 wt % reversible hydrogen capacity fixed by the U.S. Department of Energy.[6] Hence, it is necessary to explore other promising complex hydrides.

Complex lithium beryllium hydrides such as $LiBeH_3$, Li_2BeH_4, Li_3BeH_5, $LiBe_2H_5$, and $Li_3Be_2H_7$ are promising candidates because they have a higher theoretical GHD beyond 14.0 wt % H.[7–13] Zaluska *et al.*[10,11] found experimentally that compared to other known metal hydrides, lithium-beryllium hydrides show higher reversible hydrogen capacity (more than 8 wt % H near 250 °C). Based on the x-ray diffraction (XRD) results, it is expected that the adsorption/desorption of hydrogen proceeds according to the following reversible reaction:

$$n\mathrm{LiH} + m\mathrm{Be} + m\mathrm{H_2} \rightleftharpoons \mathrm{Li}_n\mathrm{Be}_m\mathrm{H}_{n+2m}.$$

According to Eq. (1), Li–Be hydrides can be formed with different $n:m$ molar ratios. In our present work we focus our interest on the $LiBeH_3$ system. Lipinska-Kalita *et al.*[12] investigated the crystal structure of $LiBeH_3$ using the synchrotron-radiation XRD technique and concluded that $LiBeH_3$ has a monoclinically distorted perovskite-type structure with space group $C2/c$. However, important structural details concerning the distribution of Li, Be, and H and their local coordination environments still remain unresolved. In fact, with the present experimental techniques, it is difficult to characterize these complex Li–Be hydrides. One reason, already mentioned in Refs. 10 and 11, is that the presence of impurities and oxidation products leads to very complex XRD patterns. An even more important reason is that due to the low XRD

a)Electronic mail: chaohao.hu@guet.edu.cn.

form factors of light atoms, it is difficult to determine their coordinates with sufficient precision if only x-ray data are available, requiring the availability of rather massive and preferably deuterated samples.[13] Hence, although the Li–Be hydrides have been investigated experimentally for a long time since their discovery by Bell and Coates[7] in 1968, due to little progress in sample preparation during the past 40 years, even the exact composition of these complex compounds is still an open issue. Recently Bulychev *et al.*[13] solved the structure of Li_2BeD_4 from XRD and neutron-powder diffraction data. The structure contains BeD_4 tetrahedra, and Li atoms are located in the interstices. On the basis of an analysis of the electron localization functions a strong covalent bonding within the $[BeD_4]^{2-}$ complex anions and a predominantly ionic $Li^+-[BeD_4]^{2-}$ bonding have been suggested.

Ab initio calculations based on density-functional theory (DFT) have been widely used to successfully compare the energetics of selected hypothetical and real crystal structures of various materials.[14–16] However, in this approach the completeness of the structure database is essential for the reliability of the final prediction. On the other side, being entirely different from the so-called blind test, various global minimum search methods such as simulated annealing,[17,18] metadynamics,[19,20] and evolutionary algorithms[21–23] (EAs) have been put forward to solve the crystal structure even without any experimental data.

Although the experimental crystallographic information is scarce, the structural and electronic properties of Li–Be hydrides, and especially of $LiBeH_3$, have also been successively investigated.[24–32] Starting from a proposed cubic perovskite structure, it has been proposed that $LiBeH_3$ could be a semiconductor with a small indirect energy gap or a metallic phase, eventually even a potential high-T_c superconductor.[24,25,29] Martins[27,28] found that an orthorhombic $CuGeO_3$-type structure with space group *Pmma* is more stable and an insulator with a band gap about 1.9 eV. Recently, based on DFT total-energy calculations for a larger structure database, Vajeeston *et al.*[32] predicted that at ambient conditions $LiBeH_3$ crystallizes in a $NaCoF_3$-type perovskite-related orthorhombic structure with space group *Pnma* and consists of corner-sharing BeH_6 octahedra.

However, in our opinion, the set of candidate crystal structures used in these early calculations is far from complete. The abundance in experimental crystallography data allows us to build a more complete structure database, and the increased efficiency of modern *ab initio* DFT methods allows us to build far more candidate structures in the test. Following our previous investigations on complex alkali beryllium hydrides Li_2BeH_4 (Ref. 33) and Na_2BeH_4,[34] we predict alternative ground-state crystal structures for $LiBeH_3$ and temperature- and pressure-induced phase transitions to different high-temperature and high-pressure phases. Our investigations are based on a much larger structure database (containing, in particular, all previously proposed equilibrium structures) and total-energy, electronic-structure, and phonon calculations based on DFT. On the other hand, we have used the global optimization method based on an EA to search for alternative candidate structures. The *ab initio* DFT calculations have also been used to investigate the adsorption/desorption properties of $LiBeH_3$.

II. COMPUTATIONAL DETAILS

The *ab initio* DFT calculations were performed within generalized gradient approximation to the exchange-correlation functional as parametrized by Perdew and Wang[35] and using a plane-wave method as implemented in the Vienna *ab initio* simulation package (VASP).[36] VASP performs a solution of the Kohn–Sham equations of DFT using efficient iterative diagonalization techniques and charge-density mixing routines. The projector augmented wave (PAW) scheme[37,38] was used to describe the electron-ion interaction. A kinetic energy cutoff with 400 eV was used in all calculations. The atomic positions, lattice parameters, and cell volume were fully optimized using conjugate-gradient and quasi-Newton techniques until total energy is converged to within 0.1 meV and the forces on all atoms are smaller than 1 meV/Å. To achieve a high accuracy of the Brillouin-zone integration, dense *k*-point grids with a *k*-point spacing smaller than 0.03 $Å^{-1}$ was used for all structures.

A search for the equilibrium crystal structure of $LiBeH_3$ was also performed using an *ab initio* EA as implemented in the USPEX (universal structure predictor: evolutionary xtallography) code.[21–23] In USPEX, utilizing the free energy calculated from an *ab initio* code as fitness function, new stable crystal structures can successfully be predicted in the absence of any experimental information. In the present work, variable-cell simulations for systems containing *N* atoms in the primitive cell (here, $N=10$, 15, and 20) were performed using no experimental data. In addition, evolutionary simulations based on the experimental lattice parameters from Ref. 12 were also carried out. During simulations, no symmetry constraints were imposed, and therefore the resulting structures are guaranteed to have no elastic instabilities and no soft modes at the center of the Brillouin zone. The first generation of structures was produced randomly and the succeeding generations were obtained by applying heredity, mutation, and permutation operations, with probabilities of 60%, 20%, and 10%, respectively, to the lowest-energy of 60% of each generation. More details about EA simulations can be found in Refs. 22 and 23. At the postprocessing stage, the symmetry of various structures from EA simulations was identified using the ISOTROPY package.[39]

To determine the temperature-dependent free energy of $LiBeH_3$, the phonon density of states was calculated from the "direct" approach,[40–42] which is based on the supercell calculations of the interatomic force constants, relying on the forces calculated using VASP. To calculate the force constants for $LiBeH_3$, atomic displacement amplitudes of 0.01 Å were used. The $2\times2\times1$, $2\times2\times2$, $1\times1\times2$, $1\times2\times3$, $1\times2\times1$, $1\times3\times2$, and $2\times2\times2$ supercells were used for α-$LiBeH_3$, $CaSiO_3$_2-type, $MgSiO_3$-type, $BaSiO_3$-type, YBO_3-type, USPEX_1, and USPEX_2 structures (the nomenclature is explained below), containing 240, 240, 80, 120, 120, 120, and 160 atoms per cell, respectively.

TABLE I. Calculated volume V_0 (Å^3/f.u.) and energy difference ΔE_0 (meV/f.u.) of possible $LiBeH_3$ phases from *ab initio* total-energy calculations. CN_{Be} is the H coordination number of Be atoms in various candidates.

Prototype	Space group	Z	CN_{Be}	V_0 (Å^3/f.u.)	ΔE_0 (meV/f.u.)
$CaSiO_3$_1	$P2_1/c$	12	4	39.896	0
$CaSiO_3$_2	P-1	6	4	39.890	4.9
YBO_3	$Cmcm$	12	4	40.461	36.1
$MgSiO_3$	$C2/c$	8	4	38.161	72.5
$InAlS_3$	$P6_1$	6	4	42.413	77.3
$CdPS_3$	$C2/m$	4	4	49.179	84.7
$BaSiO_3$	$P2_12_12_1$	4	4	39.352	87.6
$LiPO_3$	$P2/c$	20	4	43.466	122.3
$CsBeF_3$	$Pnma$	4	4	40.822	189.5
$NaPO_3$	$I4_1/a$	16	4	42.178	238.7
$CuGeO_3$_1	$P2_12_12$	16	4	40.451	314.1
$CuGeO_3$_2	$Pbam$	16	4	40.209	315.2
$CuGeO_3$_3	$Pmma$	2	4	41.097	333.7
$CuGeO_3$_4	$Cmca$	8	4	40.847	334.1
$GdBO_3$	$R32$	18	4	42.542	359.8
$SrGeO_3$	P-62m	3	4	43.041	360.8
$NaCoF_3$	$Pnma$	4	6	30.688	531.3
$BaPbO_3$	$Imma$	4	6	30.905	565.7
$KMgH_3$	Pm-3m	1	6	31.599	615.1
$BaTiO_3$_1	$P4mm$	1	6	31.371	615.2
$BaTiO_3$_2	$Amm2$	2	6	31.570	616.6
$BaTiO_3$_3	$R3m$	1	6	31.263	616.5
$CsMgH_3$_1	R-3m	9	6	33.042	672.1
$CsMgH_3$_2	$Pmmn$	6	6	35.132	725.1

III. RESULTS AND DISCUSSION

A. Geometric structures from total-energy calculations

Ab initio total-energy calculations for $LiBeH_3$ in 24 different potential structures with ABX_3 stoichiometry have been performed. When more than one structures with different space groups exist for a compound with the same chemical composition, the structures are labeled as "_1," "_2," "_3," etc. The proposed structures for $LiBeH_3$ include $KMgH_3$,[43] $CsMgH_3$_1,[44] $CsMgH_3$_2,[45] $CsBeF_3$,[46] $NaCoF_3$,[47] $CaSiO_3$_1,[48] $CaSiO_3$_2,[48] $MgSiO_3$,[48] $CaGeO_3$,[48] $BaSiO_3$,[49] $CuGeO_3$_1,[50] $CuGeO_3$_2,[50] $CuGeO_3$_3,[51] $CuGeO_3$_4,[52] $SrGeO_3$,[53] $BaTiO_3$_1,[54] $BaTiO_3$_2,[54] $BaTiO_3$_3,[54] $BaPbO_3$,[55] $NaPO_3$,[56] $LiPO_3$,[57] YBO_3,[58] $GdBO_3$,[59] $InAlS_3$,[60] and $CdPS_3$.[61] Compared to the structure database used by Vajeeston *et al.*,[32] most candidates from ternary halides have been excluded, except for the $NaCoF_3$-type structure which has been found to be most stable in the their work.[32] Structures from silicates, alkali-metal-beryllium fluorides, and phosphates which had been neglected in previous studies are strongly represented in our present work, since many BX_4 tetrahedra (e.g., SiO_4, BeF_4, and PO_4) are found in these structures. This is motivated by the fact that recent x-ray powder-diffraction experiments on $LiBeH_3$ (Ref. 12) and Li_2BeH_4 (Ref. 13) have shown that the BeH_4 tetrahedra are the basic building blocks and Li atoms are located in the interstices of Li–Be hydrides.

The optimized volumes (V_0) and the ground-state energy differences (ΔE_0) per f.u. for these hypothetical structures are summarized in Table I, and some crystal structures with low ΔE_0 (about a few tens of meV/f.u.) are depicted in Fig. 1. As listed in Table I, the $CaSiO_3$_1-type structure with space group $P2_1/c$ (hereafter α-$LiBeH_3$) has the lowest total energy, indicating that it is the energetically most favorable structure within the present structure database. The $CaSiO_3$_2-type structure with space group P-1 is energetically almost degenerate with α-$LiBeH_3$, with only 4.9 meV/f.u. energy difference. As shown in Fig. 1, the two lowest-energy structures all contain BeH_4 tetrahedra linked in zigzag chains (corner-sharing tetrahedral with orientations alternating in a 2:1 sequence–chain I as depicted in the inset of Fig. 1). Other low-energy structures from the silicate family are the $MgSiO_3$-type structure with space group $C2/c$ and the $BaSiO_3$-type structure with space group $P2_12_12_1$. In these structures, the BeH_4 tetrahedra are also linked in zigzag chains (alternating in a 1:1 sequence–chain II as depicted in the inset of Fig. 1). Phases isostructural to alkali-metal phosphates such as $NaPO_3$ and $LiPO_3$ are higher in energy by 122.3 and 238.7 meV/f.u., respectively. Also the $CdPS_3$-type, $InAlS_3$-type, and YBO_3-type structures which do not belong to any of the structural families discussed above are less stable than α-$LiBeH_3$ by 84.7, 77.3, and 36.1 meV/f.u. only. In the $CdPS_3$-type and YBO_3-type structures the BeH_4 tetrahedra are linked in pair or triangle rings, as presented in the inset of Fig. 1. The $NaCoF_3$-type structure with space group $Pnma$ containing the BeH_6 octahedra is energetically unfavorable, with ΔE_0=531.3 meV/f.u. The $CsBeF_3$-type structure is more stable than the $NaCoF_3$-type structure by 341.8 meV/f.u., although they belong to the same space group. In fact, similar to the $MgSiO_3$-type structure, the local atomic

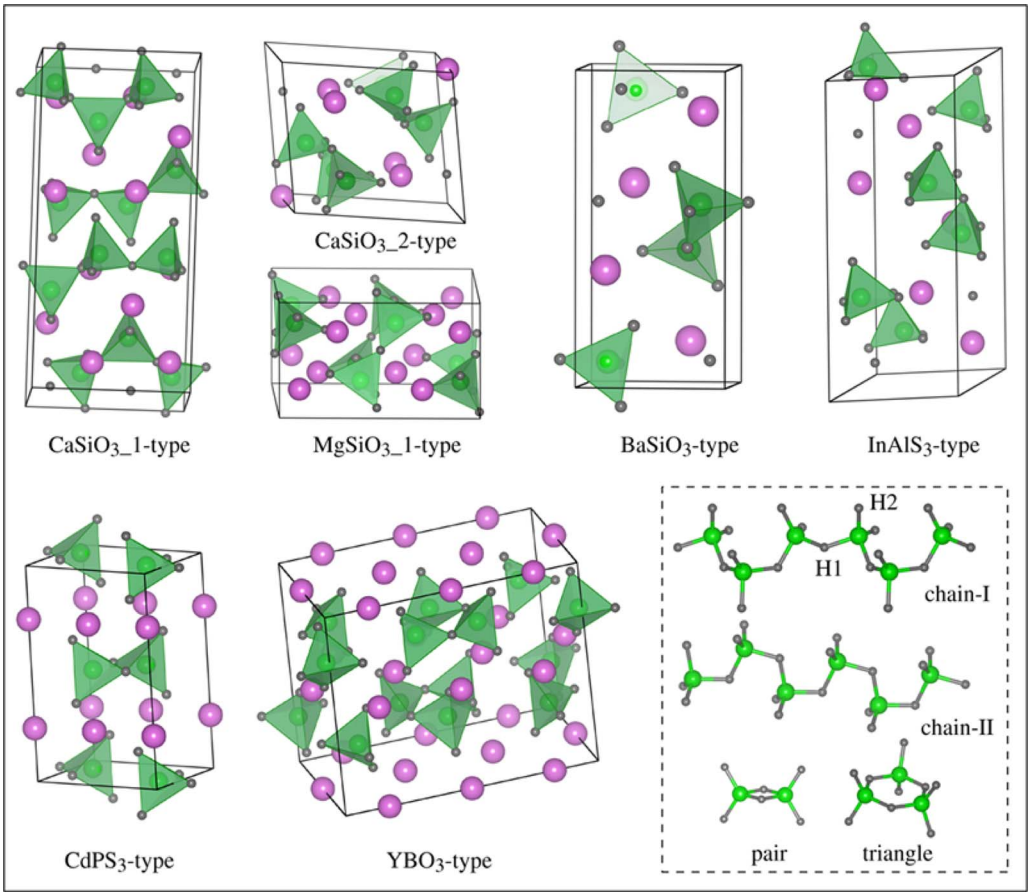

FIG. 1. (Color online) Crystal structure of competing $LiBeH_3$ phases predicted from total-energy calculations: $CaSiO_3$_1 type (ground state, α-$LiBeH_3$) (monoclinic, $P2_1/c$), $CaSiO_3$_2 type (triclinic, P-1), $MgSiO_3$ type (monoclinic, $C2/c$), $BaSiO_3$ type (orthorhombic, $P2_12_12_1$), $InAlS_3$ type (trigonal, $P6_1$), $CdPS_3$ type (monoclinc, $C2/m$), and YBO_3 type (orthorhombic, $Cmcm$) structures. The corner-sharing BeH_4 tetrahedra are linked in type-I and type-II zigzag chains or form edge-sharing pairs and/or triangular rings as shown in the inset. Hydrogen atoms in bridging position or at isolated vertices are marked H1 and H2, respectively.

arrangement of the $CsBeF_3$-type structure is based on the BeH_4 tetrahedra linked in chain II and hence entirely different from the $NaCoF_3$-type structure. This confirms that in $LiBeH_3$, the BeH_4 tetrahedra linked in chains and not the BeH_6 octahedra are constituent building blocks. This is not too surprising because it is well known that in the structure of BeH_2, the BeH_4 tetrahedra form even extended networks. The change in connectivity of the tetrahedral building blocks from networks to chains or rings is directly related to the variation in the stoichiometric composition of crystal. It can be expected that the coordination of the tetrahedral is further reduced from chains or rings to isolated BeH_4 subunits if the Li content is increased,[62] as shown for Li_2BeH_4.[13] To facilitate the following discussion, we distinguish between hydrogen atoms located in corners shared between the BeH_4 tetrahedra (bridging H1 atoms) and "normal" H2 atoms bond to only one Be atom (as marked in the inset of Fig. 1).

The optimized structural parameters for α-$LiBeH_3$, $CaSiO_3$_2-type, $MgSiO_3$-type, and YBO_3-type structures are presented in Table II. Each Be atom is coordinated by four H atoms in slightly distorted tetrahedra. The bond length between Be and a bridging H1 atom (L_{Be-H1}) is distinctly longer than that between Be and a H2 atom (L_{Be-H2}). For example, the average L_{Be-H1} bond lengths in α-$LiBeH_3$ and in the $MgSiO_3$-type and YBO_3-type structures are 1.433, 1.476, and 1.425 Å and the corresponding L_{Be-H2} bond lengths are 1.406, 1.407, and 1.399 Å, respectively. The same effect (even more pronounced) is known for silicates and was recently predicted for tetrahedral carbonates.[63] However, we must point out here that the proposed structures based on newly predicted phases of $MgCO_3$ from Ref. 63 are noticeably higher in energy than α-$LiBeH_3$, although they have very similar building blocks. The number of H atoms around Li atoms varies in these competing phases owing to different building blocks (chains versus rings), and the variation in bond length between Li and H (L_{Li-H}) is in a rather large range. For example, each Li atom is coordinated by six H atoms and L_{Li-H} varies from 1.876 to 2.140 Å in α-$LiBeH_3$ and from 1.840 to 1.956 Å in the $MgSiO_3$-type structure. In the YBO_3-type structure, each Li atom is coordinated by eight H atoms and L_{Li-H} is longer and ranges from 1.936 to 2.236 Å. In addition, the Be–H1–Be angles in these competing structures are also different, about 129.3°, 134.4°, and 120.7° for α-$LiBeH_3$, $MgSiO_3$-type, and YBO_3-type structures, respectively.

B. Structures obtained by evolutionary simulations

The energetically most favorable structures determined in the preceding section contain between 6 and 12 f.u., i.e.,

TABLE II. Optimized structural parameters of competing $LiBeH_3$ phases from *ab initio* total-energy calculations.

Prototype	Lattice constants (Å)		Internal atomic positions		
			x	y	z
$CaSiO_3$_1 ($P2_1/c$)	a=6.0138	Li1:	0.010 34	0.119 05	0.247 76
	b=6.1251	Li2:	0.239 13	0.882 27	0.406 84
	c=13.1242	Li3:	0.252 56	0.372 37	0.399 02
	β=82.3646	Be1:	0.228 30	0.593 47	0.587 61
		Be2:	0.224 08	0.165 47	0.591 60
		Be3:	0.565 45	0.117 80	0.313 56
		H1:	0.330 48	0.119 11	0.305 98
		H2:	0.291 76	0.617 12	0.281 55
		H3:	0.026 54	0.644 35	0.651 74
		H4:	0.025 41	0.120 17	0.658 92
		H5:	0.225 24	0.623 62	0.481 59
		H6:	0.197 21	0.130 91	0.489 30
		H7:	0.423 05	0.695 35	0.619 74
		H8:	0.425 00	0.064 48	0.617 44
		H9:	0.292 87	0.380 09	0.616 11
$CaSiO_3$_2 (P-1)	a=6.0044	Li1:	0.989 29	0.248 27	0.004 45
	b=6.1264	Li2:	0.253 13	0.927 01	0.297 22
	c=6.7632	Li3:	0.238 50	0.432 17	0.315 19
	α=76.0122	Be1:	0.772 29	0.952 23	0.325 15
	β=82.8140	Be2:	0.775 15	0.382 10	0.316 85
	γ=90.3877	Be3:	0.565 11	0.717 56	0.127 20
		H1:	0.670 24	0.277 10	0.888 27
		H2:	0.708 04	0.770 61	0.937 36
		H3:	0.027 25	0.062 82	0.805 38
		H4:	0.025 13	0.536 99	0.816 09
		H5:	0.221 12	0.133 62	0.463 23
		H6:	0.199 87	0.636 76	0.478 28
		H7:	0.423 86	0.136 33	0.734 87
		H8:	0.425 11	0.504 09	0.739 03
		H9:	0.294 47	0.820 38	0.730 99
$MgSiO_3$ ($C2/c$)	a=8.6656	Li1:	0.000 00	0.900 22	0.250 00
	b=8.0065	Li2:	0.000 00	0.287 98	0.250 00
	c=4.6708	Be:	0.214 62	0.587 18	0.235 88
	β=109.5996	H1:	0.387 00	0.594 62	0.338 88
		H2:	0.136 32	0.257 54	0.657 89
		H3:	0.145 34	0.509 45	0.452 52
YBO_3 ($Cmcm$)	a=10.1207	Li1:	0.173 51	0.000 00	0.000 00
	b=5.8077	Li2:	0.500 00	0.000 00	0.000 00
	c=8.2605	Be1:	0.622 45	0.212 67	0.250 00
		Be2:	0.500 00	0.582 03	0.250 00
		H1:	0.321 29	0.155 92	0.399 50
		H2:	0.500 00	0.693 18	0.098 30
		H3:	0.121 70	0.958 00	0.250 00
		H4:	0.500 00	0.091 44	0.250 00

between 30 and 60 atoms per cell. This is definitely too large for an optimization via EA. However, we have applied the EA to smaller cells with 10 or 20 atoms to verify whether the EA converges to the same constituent building blocks. From the variable-cell evolutionary simulations, the total energy of $LiBeH_3$ including 10 and 20 atoms in the primitive cell versus generation number is presented in Fig. 2. The lowest-energy structures for each evolutionary search are illustrated in the inset and named USPEX_1 and USPEX_2, respectively. As shown in Fig. 2(a), similar to the $MgSiO_3$-type and $BaSiO_3$-type structures, the USPEX_1 structure with space group $C2$ also consists of BeH_4 tetrahedra linked in chain II. In the USPEX_2 structure with space group $P1$, the BeH_4 tetrahedra are linked in square rings as illustrated in Fig. 2(b). The evolutionary simulations based on fixed lattice parameters from experiment[12] have also been performed. Unfortunately, the most stable structure from the fixed-cell simulation is less stable than the USPEX_2 structure by

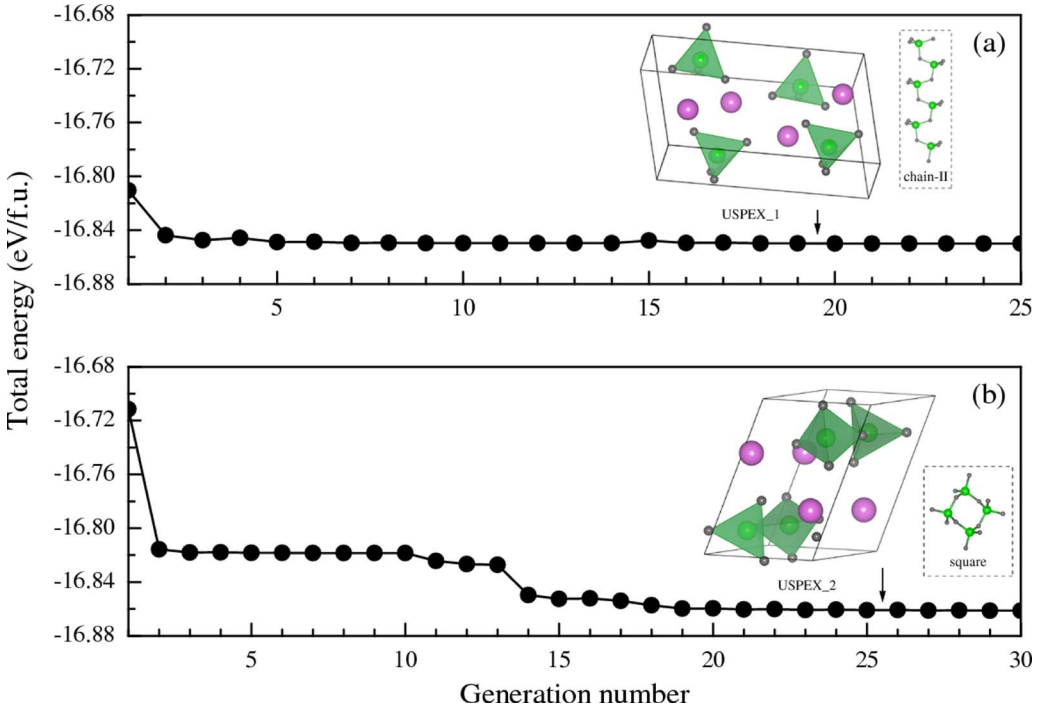

FIG. 2. (Color online) Evolution of the total energy during the *ab initio* evolutionary optimization for unit cells containing (a) 10 or (b) 20 atoms in the primitive cell. The optimized USPEX_1 (monoclinic, $C2$) and USPEX_2 (triclinic, $P1$) structures are shown in the insets. The arrangements of the BeH_4 tetrahedra linked in type-II chains for USPEX_1 and in square rings for USPEX_2 structure are also shown.

about 230 meV/f.u. and also cannot be assigned to the space group $C2/c$ (the space group suggested by Lipinska-Kalita *et al.*[12]). The optimized structural parameters of the two competing phases, together with the structural energy difference ΔE_0 with respect to α-$LiBeH_3$, are summarized in Table III. We find that the USPEX_1 and USPEX_2 structures are less stable by only about 36.7 and 21.8 meV/f.u. than α-$LiBeH_3$, which further confirms that at ambient conditions the crystal structures of $LiBeH_3$ built by the BeH_4 tetrahedra linked in chains or rings are energetically favorable, and that there are a multitude of such energetically competitive structures (which suggests that finding the global minimum using EAs and other methods may be difficult).

C. Electronic structure

The calculated electronic densities of states (EDOSs) of low-energy $LiBeH_3$ phases including α-$LiBeH_3$, YBO_3-type, and USPEX_2 structures are presented in Figs. 3(a)–3(c). To avoid redundancy the EDOSs of other structures with BeH_4 chains (e.g., $CaSiO_3$_2-type, $MgSiO_3$-type, and $BaSiO_3$-type structures) are not shown. They are similar to the EDOS of α-$LiBeH_3$, except for differences in the width of the energy band gap E_g between the valence band (VB) and conduction band. As shown in Fig. 3, the E_g of α-$LiBeH_3$ and the YBO_3-type and USPEX_2 structures are 4.84, 4.41, and 4.82 eV, respectively, which are comparable to the E_g=4.4 eV for Li_2BeH_4.[33] This shows that at ambient conditions $LiBeH_3$ is a wide-gap insulator. It is noted that our calculated E_g are distinctly larger than those calculated for the proposed $CuGeO_3$-type and $NaCoF_3$-type structures ($E_g \sim 1.9$ and 2.3 eV).[28,32] Considering the fact that the band gap of insulators and semiconductors derived from DFT calculations is consistently underestimated by approximately 30%–40% compared to experimental values, we estimate that the real E_g for $LiBeH_3$ will be at least in the order of 6 eV. Another common feature is that in the VB region the EDOS is mainly dominated by the overlapping H s and Be s,p states while the contribution from Li s,p states is much smaller. This feature suggests a predominantly ionic interaction between Li^+ cations and the $[BeH_4]^{2-}$ anion complexes, while the bonding within the tetrahedral is largely covalent. The partial EDOSs of the bridging H1 and normal H2 atoms in Fig. 3 show that H1 s states cover to the whole VB region, while the H2 s states are mainly localized in the energy region from −3.2 eV to E_f, reflecting the difference in the chemical bonding to Be atoms. The EDOSs of the YBO_3-type and USPEX_2 phases [see Figs. 3(b) and 3(c)] are distinctly different. Their VBs are divided into two and three subbands, which are directly related to the different connectivities of the BeH_4 tetrahedra. In the YBO_3-type and USPEX_2 structures the BeH_4 tetrahedra are linked in triangle and square rings as shown in Figs. 1 and 2, but the Be_3H_9 and Be_4H_{12} groups are isolated and not linked in BeH_4 chains like in α-$LiBeH_3$ and the $CaSiO_3$_2-type and $MgSiO_3$-type phases. A split VB is a common characteristic of the complex hydrides with isolated BX_4 subunits such as $NaAlH_4$,[64] $LiBH_4$,[65] $Mg(AlH_4)_2$,[66] and Li_2BeH_4.[33] A broad and continuous VB like in α-$LiBeH_3$ is closer to the electronic structure of BeH_2,[67] in which the BeH_4 tetrahedra form extended networks.

The chemical bonding in the competing $LiBeH_3$ phases has been further investigated using crystal orbital Hamilton population (COHP) analysis,[68] as implemented in the TB-LMTO-ASA program,[69] which can provide a quantitative mea-

TABLE III. Optimized structural parameters, together with ΔE_0 (relative to α-$LiBeH_3$), of the USPEX_1 and USPEX_2 structures from evolutionary simulations.

Structure	Lattice constants (Å)	Internal atomic positions	x	y	z	ΔE_0 (meV/f.u.)
USPEX_1 ($C2$)	a=9.1418	Li:	0.375 96	0.430 66	0.366 67	
	b=3.8591	Be:	0.276 78	0.377 21	0.850 81	
	c=5.1086	H1:	0.422 70	0.439 80	0.723 73	
	β=79.7890	H2:	0.176 93	0.440 47	0.671 29	
		H3:	0.234 55	0.503 91	0.116 69	36.7
USPEX_2 ($P1$)	a=4.6593	Li1:	0.754 08	0.427 86	0.632 27	
	b=6.4569	Li2:	0.946 05	0.951 35	0.650 06	
	c=6.1205	Li3:	0.103 99	0.278 15	0.278 61	
	α=96.6277	Li4:	0.295 89	0.801 58	0.296 43	
	β=106.7984	Be1:	0.436 99	0.743 61	0.755 57	
	γ=100.1679	Be2:	0.286 97	0.354 31	0.772 86	
		Be3:	0.613 33	0.485 91	0.173 12	
		Be4:	0.763 01	0.875 20	0.155 88	
		H1:	0.259 44	0.844 65	0.589 83	
		H2:	0.553 93	0.342 57	0.957 43	
		H3:	0.216 05	0.561 90	0.769 88	
		H4:	0.701 83	0.708 24	0.703 80	
		H5:	0.496 04	0.886 90	0.971 28	
		H6:	0.003 96	0.235 76	0.778 47	
		H7:	0.358 79	0.276 47	0.573 96	
		H8:	0.833 95	0.667 60	0.158 78	
		H9:	0.046 08	0.993 72	0.150 37	
		H10:	0.348 18	0.521 27	0.224 88	
		H11:	0.790 55	0.384 83	0.338 84	
		H12:	0.691 16	0.952 98	0.354 79	21.8

sure of bond strengths. In contrast to the familiar crystal orbital overlap population analysis,[70] the COHP analysis is a partitioning scheme for the band structure energy in terms of orbital-pair contributions. In all the COHP curves presented here positive and negative regions correspond to the bonding and antibonding interactions, which is opposite to the original definition.[68] The COHP curves for Be–H1, Be–H2, Li–H, and H–H bonds in α-$LiBeH_3$ and in the YBO_3-type and USPEX_2 structures are presented in Fig. 4. As expected the Be–H1 and Be–H2 interactions are predominant in the VB regions, while the Li–H and H–H interactions are very weak due to large interatomic distances. The Be–H2 interactions are bonding in the whole VB region, while the Be–H1 interactions are antibonding at lower binding energies (from −1.8, −2.6, and −2.9 eV to E_f for α-$LiBeH_3$, YBO_3-type, and USPEX_2 structures). The Be–H1 bonding interactions are concentrated at energies below −5.1 eV, reflecting a strong bonding-antibonding splitting. The COHP integrated up to E_f (ICOHP), as an indicator of the bonding strength, is also considered. The ICOHPs of Be–H1 bonds in α-$LiBeH_3$, YBO_3-type, and USPEX_2 phases are 0.84, 0.82, and 0.64 eV and the corresponding ICOHPs of Be–H2 bonds are 1.15, 1.36, and 0.84 eV. This confirms the fact that the strength of covalent Be–H2 bonds is stronger than that of Be–H1 bonds because only bonding and no antibonding states are occupied.

We also analyzed the charge transfer. The difference charge densities for α-$LiBeH_3$ and the YBO_3-type phase are shown in Fig. 5. They are calculated as the difference between the self-consistent total charge density and a superposition of atomic charge densities at the same lattice positions. We find that electrons are depleted from Li and Be sites and transferred to H sites. In addition, the charge density around H is polarized toward Be, reflecting the existence of an ionocovalent Be–H bond. Altogether this confirms the ionic bonding between Li and BeH_4 units and the strong polar covalent between Be and H in the BeH_4 complexes.

D. Vibrational properties

The total and partial phonon DOSs (PDOSs) of five competing $LiBeH_3$ phases calculated using the direct force-constant approach[40–42] are presented in Fig. 6. The basic features of the PDOS are rather similar for all structures. Three frequency ranges dominated by the vibrations of Li, Be, and H atoms may be distinguished. The first region up to about 510 cm^{-1} is almost unchanged, which corresponds to the librational modes resulting from the displacements of Li ions and BeH_4 tetrahedra. Li atoms generally do not participate in vibrations at higher frequencies. The high-frequency modes may be classified as bending modes involving fluctuations in the H–Be–H bond angles and stretching modes straining the Be–H bond length. In the high-frequency modes, the dis-

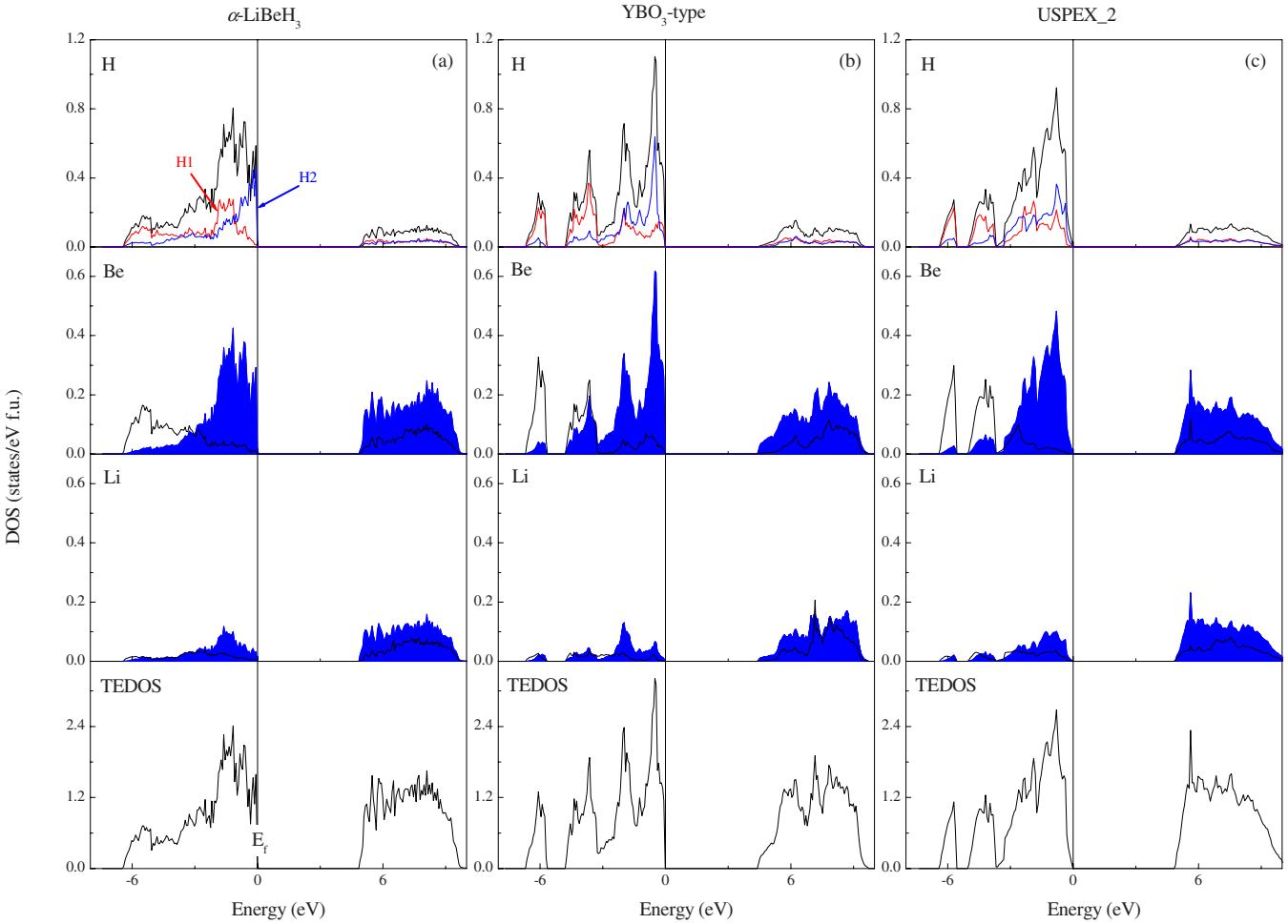

FIG. 3. (Color online) Calculated total and projected EDOSs for α-$LiBeH_3$ ($CaSiO_3$-type), YBO_3-type, and USPEX_2 structures at equilibrium. Energies are given relative to the upper edge of the VB. The PDOSs of Li and Be atoms are marked by the shaded-blue areas; the *s*-states of H1 and H2 atoms (as marked in Fig. 1) are plotted in red and blue solid lines, respectively.

placements of H and Be atoms are strongly coupled. Unlike in other complex hydrides such as $NaAlH_4$ (Ref. 71) or Na_2BeH_4,[34] the frequency ranges of libratonal and bending modes overlap in the α- and $MgSiO_3$-type phases of $LiBeH_3$. The highest frequencies of Be–H stretching modes are approximately 200 cm^{-1} higher than in Na_2BeH_4 (Ref. 34) due to the stronger Be–H interactions. Some differences in the PDOS are due to the different local arrangements of Li ions and BeH_4 tetrahedra in these competing phases. First, as shown in Fig. 6(a), the stretching modes in α-$LiBeH_3$ are shifted to higher frequencies compared to the other phases, reflecting the stronger Be–H bonding. In addition, in the $BaSiO_3$-type, YBO_3-type, and USPEX_1 structures some bending modes are splitted from the main band and shifted to higher frequency regions from 1060 to 1490 cm^{-1}. This is related to the smaller and stiffer Be–H1–Be bond angles (114.3°, 120.7°, and 116.7°) in the $BaSiO_3$-type, YBO_3-type, and USPEX_1 structures, compared to bond angles of 129.3° and 134.4° for α-$LiBeH_3$ and the $MgSiO_3$-type structure. An important point is that for the USPEX_2 structure some phonon modes have imaginary frequencies—hence, although this structure represents a local energy minimum, it is a dynamically unstable structure.

E. Structural stability and phase transitions

Now we turn to investigate the structural stability of $LiBeH_3$ under finite temperatures and pressures. The free energy (F) can be calculated in a quasiharmonic approximation.[72] The calculated free energy difference (ΔF) with respect to α-$LiBeH_3$ as a function of temperature is displayed in Fig. 7(a). At low temperatures α-$LiBeH_3$ is most stable, but a structural transition to the YBO_3-type structure occurs at $T=408$ K. From the calculated enthalpy difference (ΔH) as a function of pressure shown Fig. 7(b), we find that the $MgSiO_3$-type structure becomes lower in enthalpy than the α-$LiBeH_3$ phase at a pressure larger than 7.1 GPa. This pressure-induced structural transition from α-$LiBeH_3$ to the $MgSiO_3$-type structure is in agreement with experimental observations of phase transitions in the pressure range between 5.0 and 17.5 GPa by high-pressure Raman spectroscopy.[12] According to our calculations structures with BeH_4 tetrahedra have a lower enthalpy than structures based on BeH_6 octahedra (like the $NaCoF_3$-type structure) for pressures up to 20.0 GPa.

It is interesting to note that the pressure effect on the structure of $LiBeH_3$ is entirely different from the temperature effect. For example, with increasing pressure phases in

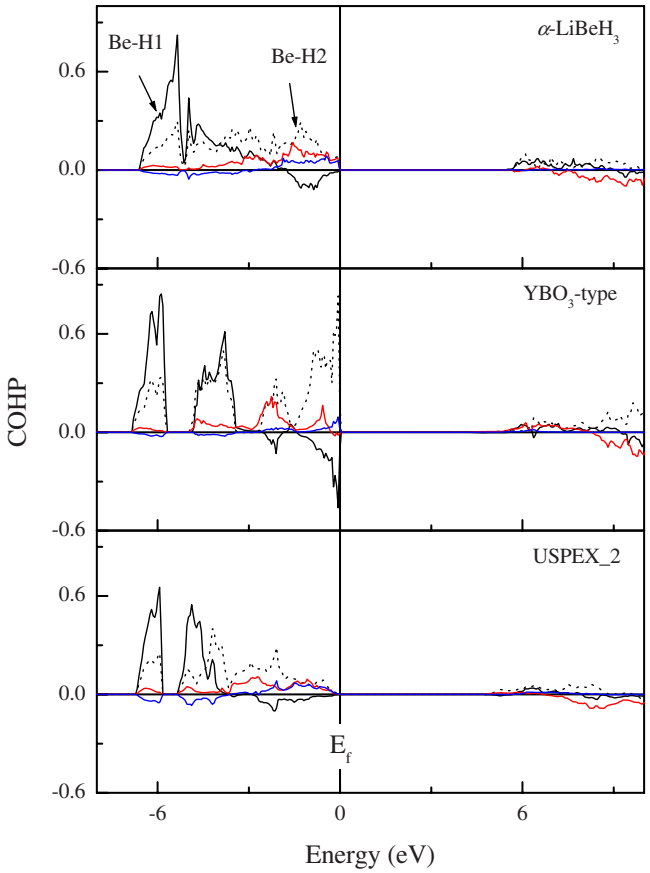

FIG. 4. (Color online) Calculated COHP analysis for α-$LiBeH_3$, YBO_3-type, and USPEX_2 structures. Energies are given relative to the upper edge of the VB. The COHP curves for Be–H1 and Be–H2 bonds are plotted in black solid and dotted lines for Li–H and H–H bonds in red and blue solid lines, respectively.

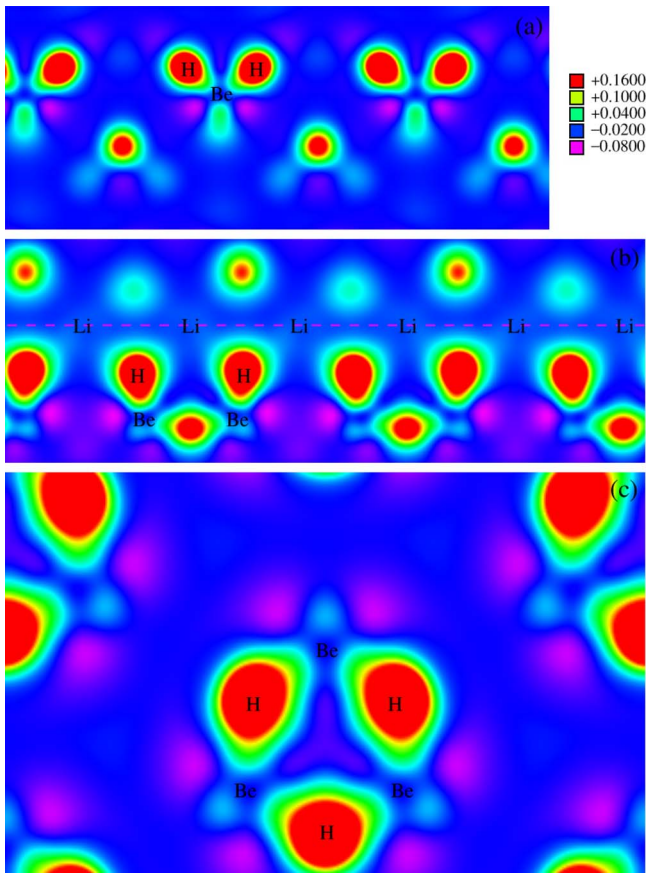

FIG. 5. (Color online) Difference charge-density distribution in $LiBeH_3$ (in $e/Å^3$): (a) Be–H1 bonding plane and (b) Be–H2 bonding plane for α-$LiBeH_3$; (c) Be–H1 bonding plane for YBO_3-type structure. Li ions in α-$LiBeH_3$ are distributed uniformly along a purple dashed line as marked in (b).

which the BeH_4 form rings like in the YBO_3-type and USPEX_2 structures are increasingly disfavored. At increasing temperature, the YBO_3-type structure is stabilized at $T > 408$ K, while the $MgSiO_3$-type high-pressure phase and the related $BaSiO_3$-type structure become energetically unfavorable. This can be understood in terms of a detailed analysis in the atomic arrangement and bonding in the competing phases. At a hypothetical pressure-induced transition from α-$LiBeH_3$ (with BeH_4 tetrahedra linked in chain I) to the YBO_3-type structure with triangular rings of the BeH_4 tetrahedra some Be–H1 bonds would have to be broken. This is out of rule because under pressure an even more compact packing of the BeH_4 tetrahedra is required. However, the excitation of librations of the tetrahedral with increasing temperature favors breaking the weaker Be–H1 bonds. As the transformation is reconstructive, we expect the transition to be rather sluggish—but an investigation of the kinetics of the transition is beyond the scope of the present work. In fact, similar phase transitions, involving bond breaking, are well known, e.g., they were experimentally seen in Ba_6Ge_{25} (Ref. 73) and in molecular dynamics simulations of aluminosilicates,[74] in which the stronger covalent Ge–Ge and Al–O bonds were broken with increasing temperature. In contrast, the pressure-induced phase transition from α-$LiBeH_3$ to the $MgSiO_3$-type structure should be rapid and displacive as no bond breaking and bond reformation are required. The Be–H1–Be linkages in the type-I and type-II chains of the competing $LiBeH_3$ phases (see Fig. 1) are rather flexible. Under pressure, the transformation from α-$LiBeH_3$ to the $MgSiO_3$-type structure can be accomplished by an almost rigid rotation of the BeH_4 tetrahedra. Pressure-

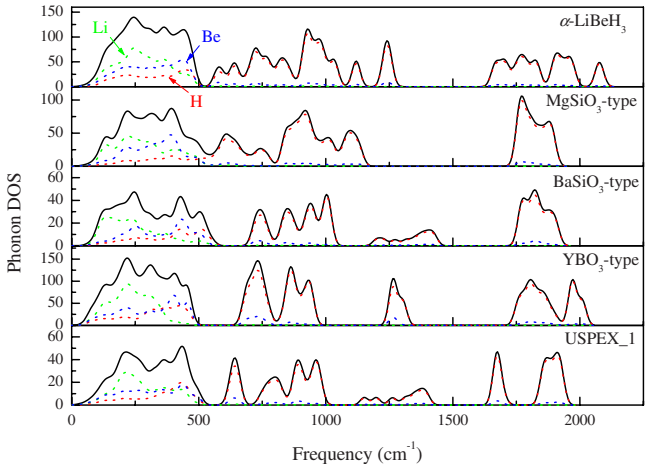

FIG. 6. (Color online) Calculated PDOS and partial PDOS for α-$LiBeH_3$, $MgSiO_3$-type, $BaSiO_3$-type, YBO_3-type, and USPEX_1 structures. The partial PDOS of H, Li, and Be are plotted in red, green, and blue dotted lines, respectively.

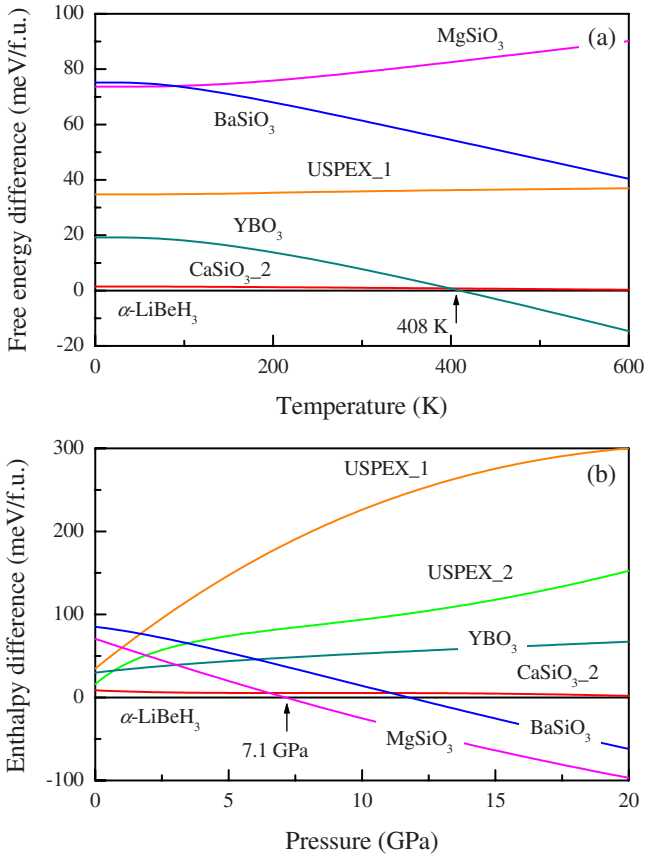

FIG. 7. (Color online) Phase stability of $LiBeH_3$: (a) Free energy difference $\Delta F=\Delta E_0+\Delta F_{vib}$ vs temperature and (b) enthalpy difference vs pressure with respect to α-$LiBeH_3$. The structural transition points induced by temperature or pressure are marked by arrows.

driven phase transitions based on the softening of "rigid unit modes" are a common feature of many framework structures such as silicates and zeolites.[75]

F. Adsorption and desorption properties of $LiBeH_3$

Finally, we further discuss the adsorption and desorption properties of $LiBeH_3$ from the enthalpy of formation (ΔH_f, in kJ/mol H_2). The calculated ΔH_f based on various reaction pathways [(i) reaction of the binary hydrides; (ii) reaction of Li hydride with metallic Be, followed by hydrogenation; (iii) reaction of Be hydride with metallic Li, followed by hydrogenation; (iv) alloying of metallic Li and Be, followed by hydrogenation] for α-$LiBeH_3$ ($CaSiO_3$-type) and a $NaCoF_3$-type phase (taken from Ref. 32) are listed in Table IV. The results show that all the reactions considered for the formation of α-$LiBeH_3$ are exothermic. In contrast, Vajeeston *et al.*[32] reported an endothermic heat of formation for the $NaCoF_3$-type phase if the reaction starts from the Li hydride [pathway (i) or (ii)]. An exothermic reaction is found only for the other two reaction channels, but the reaction leading to the formation of α-$LiBeH_3$ ($CaSiO_3$ type) is energetically favored. For scenario (ii), i.e., starting from LiH and Be and successive hydrogenation, the calculated ΔH_f is about −45.36 (−30.12) kJ/mol H_2 without (with) zero-point energy (ZPE) corrections.[76]

Pressure-composition isotherms for Li–Be hydrides

TABLE IV. Calculated enthalpy of formation (ΔH_f, in kJ/mol H_2) of α-$LiBeH_3$ ($CaSiO_3$-type) and the $NaCoF_3$-type structure according to various reaction pathways. The ΔH_f with ZPE correction is given in parentheses.

	ΔH_f (kJ/mol H_2)		
Reactions	α-$LiBeH_3$	$NaCoF_3$ type	Expt.
$LiH+BeH_2\rightarrow LiBeH_3$	−16.11(−18.01)	35.21, 28.85[a]	
$LiH+Be+H_2\rightarrow LiBeH_3$	**−45.36(−30.12)**	5.96, 8.74[a]	~−40[b]
$Li+BeH_2+1/2H_2\rightarrow LiBeH_3$	−100.52(−96.06)	−49.21, −58.89[a]	
$Li+Be+3/2H_2\rightarrow LiBeH_3$	−129.77(−108.17)	−78.46, −79.01[a]	

[a]After Vajeeston *et al.*, Ref. 12.
[b]After Zaluska *et al.*, Ref. 10.

($Li_nBe_mH_{n+2m}$) measured by Zaluska *et al.*[10] show a single plateau at a pressure of about 1 bar, independent of the $n:m$ ratio. The highest reversible hydrogen capacity is achieved for a ratio of $n:m=3:2$—corresponding either to a mixture of $LiBeH_3$ and Li_2BeH_4 hydrides or to an as yet unknown hydride. The fact that only one plateau is found in the pressure-composition isotherms suggests that only one type of hydrogen bonding undergoes reversible recycling, independent of the alloy composition—as is also confirmed by the investigations of Ashby and Prasad[77] who found identical infrared spectra for all hydrides. These findings agree with the fact that all hydrogen atoms are arranged in corner-sharing BeH_4 tetrahedra. From pressure-composition isotherms measured at different temperatures a van't Hoff plot showing the relation between equilibrium pressure and temperature may be constructed. From the slope of this plot the enthalpy of formation may be determined; the value of $\Delta H_f=-40$ kJ/mol H_2 measured for the 3:2 composition is in good agreement with our result. More importantly, the moderate ΔH_f for $LiBeH_3$ also meets the requirement that the ΔH_f should not exceed −40 kJ/mol H_2 to allow desorption of hydrogen at an operating temperature of about 90 °C.[78] In addition, it can also be concluded that the temperature required for hydrogen desorption from α-$LiBeH_3$ will be lower than that for $NaAlH_4$ and $LiBH_4$ since the heat of formation is less exothermic than in these hydrides [$NaAlH_4$: −53 kJ/mol H_2 (Ref. 3); $LiBH_4$: −69 kJ/mol H_2 (Ref. 4)]. Hence α-$LiBeH_3$ is a possible material for hydrogen storage with a low activation barrier for hydrogen desorption.

IV. CONCLUSIONS

In summary, on the basis of *ab initio* total-energy calculations for 24 possible crystal structures in an extended and revised structure database, we have proposed a novel $CaSiO_3$-type crystal structure (space group $P2_1/c$) for $LiBeH_3$. This structure is built by corner-sharing BeH_4 tetrahedra linked in zigzag chains, with the Li atoms located in the interstices. Hence the building principle of the ground-state structure of $LiBeH_3$ is similar to the structure determined experimentally by Bulychev *et al.*[13] for Li_2BeH_4 (with isolated BeH_4 tetrahedra) and by Smith *et al.*[79] for BeH_2 (where the tetrahedral forms extended networks). That BeH_4 tetrahedra are the constituent building blocks of the crystal

structure of $LiBeH_3$ has also been confirmed by global optimizations based on an EA. However, because of the very high computational effort, the evolutionary searches could be performed only on smaller unit cells so that the search could not converge to the complex crystal structure (12 f.u. or 60 atoms per cell) identified as the ground state in the more conventional approach. Still, it is important that the EAs confirm that the basic structure-building units are BeH_4 tetrahedra and not BeH_6 octahedra as previously proposed.[32]

The analysis of the electronic structure (total and partial densities of states, COHP, difference electron density) shows that α-$LiBeH_3$ is an insulator with a band gap about 4.84 eV. The chains of corner-sharing BeH_4 tetrahedra are stabilized by strong ionocovalent bonds, while the interaction between the Li^+ cations and the negatively charged Be–H chains is ionic.

The investigations of the structural stability $LiBeH_3$ have been extended to high pressures and finite temperatures (using a quasiharmonic approximation for the vibrational contributions to the free energy). At a temperature of 408 K a structural transition from α-$LiBeH_3$ to a YBO_3-type structure with space group *Cmcm* and BeH_4 tetrahedra linked in triangular rings is predicted. The transition is driven by the vibrational entropy. In the ground-state structure, librations of the BeH_4 tetrahedra are hindered by the intrachain bonds, while in the high-temperature phase free librations of the Be_3H_9 clusters formed by three corner-sharing tetrahedral are permitted. At low temperature and a pressure of $P=7.1$ GPa, α-$LiBeH_3$ undergoes a structural transition from the α-phase to a $MgSiO_3$-type structure with space group $C2/c$ and a slightly different arrangement of the BeH_4 tetrahedra in type-II chains allowing to achieve a higher packing density. Hence temperature- and pressure-induced phase transformations are driven by different mechanisms—the coexistence lines between the competing phases in the P,T-plane remain to be determined. Since increasing temperature disfavors the $MgSiO_3$-type phase [see Fig. 7(a)], we expect the critical pressure for the α-$LiBeH_3$ to $MgSiO_3$ transition to increase with temperature. The structural energy difference between α-$LiBeH_3$ and the YBO_3-type phase is almost pressure independent. As phonon frequencies harden under compression, we expect the critical temperature for the α-$LiBeH_3$ to YBO_3 transition to show a modest increase under compression.

The calculated enthalpies of formation for α-$LiBeH_3$ from the reaction of LiH with Be and subsequent hydrogenation, $\Delta H_f=-45.36$ (-30.12) kJ/mol H_2 without (with) the ZPE corrections, are in good agreement with the experimental result (−40 kJ/mol H_2). A low heat of formation also meets the requirement for polymer electrolyte membrane fuel cells that ΔH_f should not exceed −40 kJ/mol H_2 if hydrogen desorption is possible at an operating temperature of about 90 °C. This suggests that α-$LiBeH_3$ is a potential material for hydrogen storage with lower activation barriers for hydrogen desorption compared to other complex hydrides studied extensively such as $NaAlH_4$ and $LiBH_4$.

ACKNOWLEDGMENTS

The authors gratefully acknowledge Dr. A. Togo for helpful discussions on phonon calculation. This work is supported by the National Natural Science Foundation of China through Grant no. 50771095. A.R.O. and A.L. gratefully acknowledge funding from the Swiss National Science Foundation (Grant Nos. 200021-111847/1 and 200021-116219) and access to the Skif MSU supercomputer (Moscow State University) and supercomputers at the Swiss Supercomputer Centre (CSCS, Manno).

[1] L. Schlapbach and A. Züttel, Nature (London) **414**, 353 (2001).
[2] B. Bogdanovic and M. Schwickardi, J. Alloys Compd. **253–254**, 1 (1997).
[3] B. Bogdanovic, R. A. Brand, A. Marjanovic, M. Schwikardi, and J. Tölle, J. Alloys Compd. **302**, 36 (2000).
[4] A. Züttel, P. Wenger, S. Rentsch, P. Sufsn, Ph. Mauron, and Ch. Emmenegger, J. Power Sources **118**, 1 (2003).
[5] Z. Lodziana and T. Vegge, Phys. Rev. Lett. **93**, 145501 (2004).
[6] Multi-Year Research, Development and Demonstration Plan: Planned Program Activities for 2005–2015, Energy Efficiency and Renewable Energy, U.S. Department of Energy. (http://www1.eere.energy.gov/hydrogenandfuelcells/mypp/pdfs/storage.pdf).
[7] A. Bell and G. E. Coates, J. Chem. Soc. A **1968**, 628 (1968).
[8] A. W. Overhauser, Phys. Rev. B **35**, 411 (1987).
[9] J. P. Bastide, Solid State Commun. **74**, 355 (1990).
[10] A. Zaluska, L. Zaluski, and J. O. Ström-Olsen, J. Alloys Compd. **307**, 157 (2000).
[11] A. Zaluska, L. Zaluski, and J. O. Ström-Olsen, Appl. Phys. A: Mater. Sci. Process. **72**, 157 (2001).
[12] K. E. Lipinska-Kalita, Y. Song, Y. Ding, J. F. Lin, M. Somayazulu, P. Dera, J. L. Yarger, H. K. Mao, and R. J. Hemley, Advanced Photon Source, Argonne National Laboratory, 2004; see http://www.aps.anl.gov/apsar2003/KRISL1.pdf.
[13] B. M. Bulychev, R. V. Shapanchenko, E. V. Antipov, D. V. Sheptyakov, S. N. Bushmeleva, and A. M. Balagurov, Inorg. Chem. **43**, 6371 (2004).
[14] Y. Liu and M. L. Cohen, Science **245**, 841 (1989).
[15] B. Magyari-Köpe, V. Ozoliņš, and C. Wolverton, Phys. Rev. B **73**, 220101(R) (2006).
[16] C. Wolverton and V. Ozoliņš, Phys. Rev. B **75**, 064101 (2007).
[17] J. Pannetier, J. Bassasalsina, J. Rodriguez-Carvajal, and V. Caignaer, Nature (London) **346**, 343 (1990).
[18] J. C. Schön and M. Jansen, Angew. Chem., Int. Ed. Engl. **35**, 1287 (1996).
[19] R. Martoňák, A. Laio, and M. Parrinello, Phys. Rev. Lett. **90**, 075503 (2003).
[20] R. Martoňák, A. Laio, M. Bernasconi, C. Ceriani, P. Raiteri, F. Zipoli, and M. Parrinello, Z. Kristallogr. **220**, 489 (2005).
[21] A. R. Oganov, C. W. Glass, and S. Ono, Earth Planet. Sci. Lett. **241**, 95 (2006).
[22] A. R. Oganov and C. W. Glass, J. Chem. Phys. **124**, 244704 (2006).
[23] C. W. Glass, A. R. Oganov, and N. Hansen, Comput. Phys. Commun. **175**, 713 (2006).
[24] M. Gupta and A. Percheron-Guegan, J. Phys. F: Met. Phys. **17**, L201 (1987).
[25] M. R. Press, B. K. Rao, and P. Jena, Phys. Rev. B **38**, 2380 (1988).
[26] R. Yu and P. K. Lam, Phys. Rev. B **38**, 3576 (1988).
[27] J. L. Martins, Bull. Am. Phys. Soc. **33**, 709 (1988).
[28] J. L. Martins, Phys. Rev. B **38**, 12776 (1988).
[29] M. Seel, A. B. Kunz, and S. Hill, Phys. Rev. B **39**, 7949 (1989).
[30] P. K. Khowash, B. K. Rao, T. McMullen, and P. Jena, Phys. Rev. B **55**, 1454 (1997).
[31] M. Li, Int. J. Quantum Chem. **68**, 415 (1998).
[32] P. Vajeeston, P. Ravindran, and H. Fjellvåg, Inorg. Chem. **47**, 508 (2008).
[33] C. H. Hu, D. M. Chen, Y. M. Wang, D. S. Xu, and K. Yang, Phys. Rev. B **75**, 224108 (2007).
[34] C. H. Hu, Y. M. Wang, D. M. Chen, D. S. Xu, and K. Yang, Phys. Rev. B **76**, 144104 (2007).
[35] J. P. Perdew and Y. Wang, Phys. Rev. B **45**, 13244 (1992).
[36] G. Kresse and J. Hafner, Phys. Rev. B **49**, 14251 (1994); G. Kresse and J. Furthmüller, Comput. Mater. Sci. **6**, 15 (1996).

[37] P. E. Blöchl, Phys. Rev. B **50**, 17953 (1994).
[38] G. Kresse and D. Joubert, Phys. Rev. B **59**, 1758 (1999).
[39] H. T. Stokes and D. M. Hatch, http://stokes.byu.edu/isotropy.html.
[40] G. Kresse, J. Furthmüller, and J. Hafner, Europhys. Lett. **32**, 729 (1995).
[41] K. Parlinski, Z. Q. Li, and Y. Kawawoe, Phys. Rev. Lett. **78**, 4063 (1997).
[42] A. Togo, http://fropho.sourceforge.net/.
[43] H. H. Park, M. Pezat, B. Darriet, and P. Hagenmuller, Rev. Chim. Miner. **24**, 525 (1987).
[44] B. Bertheville, P. Fischer, and K. Yvon, J. Alloys Compd. **330–332**, 152 (2002).
[45] G. Renaudin, B. Bertheville, and K. Yvon, J. Alloys Compd. **353**, 175 (2003).
[46] H. Steinfink and G. D. Brunton, Acta Crystallogr., Sect. B: Struct. Crystallogr. Cryst. Chem. **24**, 807 (1968).
[47] B. Lütgert and D. Babel, Z. Anorg. Allg. Chem. **616**, 133 (1992).
[48] R. T. Downs and M. H. Wallace, Am. Mineral. **88**, 247 (2003).
[49] H. P. Grosse and E. Tillmanns, Cryst. Struct. Commun. **3**, 603 (1974).
[50] M. Hidaka, M. Hatae, I. Yamada, M. Nishi, and J. Akimitsu, J. Phys.: Condens. Matter **9**, 809 (1997).
[51] S. Bräuninger, U. Schwarz, M. Hanfland, T. Zhou, R. K. Kremer, and K. Syassen, Phys. Rev. B **56**, R11357 (1997).
[52] M. Braden, G. Wilkendorf, J. Lorenzana, M. Ain, G. J. McIntyre, M. Behruzi, G. Heger, G. Dhalenne, and A. Revcolevschi, Phys. Rev. B **54**, 1105 (1996).
[53] W. Hilmer, Kristallografiya **7**, 704 (1962).
[54] G. H. Kwei, A. C. Lawson, S. J. L. Billinge, and S. W. Cheong, J. Phys. Chem. **97**, 2368 (1993).
[55] S. M. Moussa, B. J. Kennedy, and T. Vogt, Solid State Commun. **119**, 549 (2001).
[56] A. Immirzi and W. Porzio, Acta Crystallogr., Sect. B: Struct. Crystallogr. Cryst. Chem. **38**, 2788 (1982).
[57] J. C. Guitel and I. Tordjman, Acta Crystallogr., Sect. B: Struct. Crystallogr. Cryst. Chem. **32**, 2960 (1976).
[58] P. E. D. Morgan, P. J. Carroll, and F. F. Lange, Mater. Res. Bull. **12**, 251 (1977).
[59] M. Ren, J. H. Lin, Y. Dong, L. Q. Yang, M. Z. Su, and L. P. You, Chem. Mater. **11**, 1576 (1999).
[60] M. Schulte-Kellinghaus and V. Krämer, Acta Crystallogr., Sect. B: Struct. Crystallogr. Cryst. Chem. **35**, 3016 (1979).
[61] F. Boucher, M. Evain, and R. Brec, Acta Crystallogr., Sect. B: Struct. Sci. **51**, 952 (1995).
[62] In fact, according to our total-energy calculations on smaller structure databases, other lithium beryllium hydrides are also considered. The $BaSi_2O_5$-type structure with space group *Pnma*, K_3BeF_5-type structure with space group $P4/ncc$, and $Ca_3Si_2O_7$-type structure with space group *Ima*2 are found to be energetically favorable for $LiBe_2H_5$, Li_3BeH_5, and $Li_3Be_2H_7$, in which the BeH_4 tetrahedra are isolated.
[63] A. R. Oganov, S. Ono, Y. M. Ma, C. W. Glass, and A. Garcia, Earth Planet. Sci. Lett. **273**, 38 (2008).
[64] A. Aguayo and D. J. Singh, Phys. Rev. B **69**, 155103 (2004).
[65] K. Miwa, N. Ohba, and S. Towata, Phys. Rev. B **69**, 245120 (2004).
[66] C. H. Hu, D. M. Chen, Y. M. Wang, D. S. Xu, and K. Yang, J. Phys.: Condens. Matter **19**, 176205 (2007).
[67] P. Vajeeston, P. Ravindran, A. Kjekshus, and H. Fjellvåg, Appl. Phys. Lett. **84**, 34 (2004).
[68] R. Dronskowski and P. E. Blöchl, J. Phys. Chem. **97**, 8617 (1993); F. Boucher and R. Rousseau, Inorg. Chem. **37**, 2351 (1998).
[69] O. Jepsen and O. K. Andersen, TB-LMTO-ASA program, Version 4.7, MPI für Festkörperforschung, Stuttgart, Germany, 2000.
[70] R. Hoffmann, Rev. Mod. Phys. **60**, 601 (1988).
[71] A. Peles and M. Y. Chou, Phys. Rev. B **73**, 184302 (2006).
[72] J. A. Reissland, *The Physics of Phonons* (Wiley, New York, 1973).
[73] W. Carrillo-Cabrera, H. Borrmann, S. Paschen, M. Baenitz, F. Steglich, and Y. Grin, J. Solid State Chem. **178**, 715 (2005).
[74] C. Ceriani, A. Laio, E. Fois, A. Gamba, R. Martoňák, and M. Parrinello, Phys. Rev. B **70**, 113403 (2004).
[75] G. Kostorz, *Phase Transformations in Materials* (Wiley-VCH, Weinheim, 2001).
[76] From the force-constant calculations based on direct approach and supercells containing 240, 54, 72, 27, and 36 atoms, the corresponding ZPEs of α-$LiBeH_3$, LiH, BeH_2, Li, and Be are 0.766, 0.240, 0.545, 0.038, and 0.096 eV/f.u., respectively. The ZPE of H_2 is 0.271 eV calculated in a rectangular box with dimensions of $16\times14\times14$ $Å^3$.
[77] E. C. Ashby and H. S. Prasad, Inorg. Chem. **14**, 2869 (1975).
[78] F. Schüth, B. Bogdanovic, and M. Felderhoff, Chem. Commun. (Cambridge) **20**, 2249 (2004).
[79] G. S. Smith, Q. C. Johnson, D. K. Smith, D. E. Cox, R. L. Snyder, and R.-S. Zhou, Solid State Commun. **67**, 491 (1988).